Supporting Information: Within-Day Variability of SARS-CoV-2 RNA in Municipal Wastewater Influent During Periods of Varying COVID-19 Prevalence

Aaron Bivins[1,2], Devin North[1], Zhenyu Wu[1], Marlee Shaffer[1], Warish Ahmed[3], Kyle Bibby[1,2]*

[1] Department of Civil & Environmental Engineering & Earth Sciences, University of Notre Dame, 156 Fitzpatrick Hall, Notre Dame, IN 46556

[2] Environmental Change Initiative, University of Notre Dame, 721 Flanner Hall, Notre Dame, IN 46556

[3] CSIRO Land and Water, Ecosciences Precinct, 41 Boggo Road, Qld 4102, Australia

*kbibby@nd.edu

17 pages, 2 tables, 15 figures

Table S1 | RT-ddPCR assays used to detect and quantify SARS-CoV-2 RNA, PMMoV RNA, and BRSV RNA in primary influent wastewater samples. The assay used to quantify the extraction and molecular control Hep G armored RNA is also summarized.

Virus	Gene Target		Sequences	RT-ddPCR Reaction Concentration	Thermal Cycling Conditions
SARS-CoV-2	N1	F	5'-GAC CCC AAA ATC AGC GAA AT-3'	1000 nM	50°C 60 min; 95°C 10 min; 40 Cycles: 95°C 30 s, 59°C 60 s 98°C 10 min; 4°C hold
		R	5'-TCT GGT TAC TGC CAG TTG AAT CTG-3'	1000 nM	
		P	5'-FAM-ACC CCG CAT TAC GTT TGG TGG ACC-BHQ1-3'	250 nM	
PMMoV (fecal indicator virus)	replicase protein	F	5'-GAG TGG TTT GAC CTT AAC GTT TGA-3'	900 nM	
		R	5'-TTG TCG GTT GCA ATG CAA GT-3'	900 nM	
		P	5'-FAM-CCT ACC GAA GCA AAT G-MGBNFQ-3'	250 nM	
BRSV (process control)	nucleoprotein	F	5'-GCA ATG CTG CAG GAC TAG GTA TAA T-3'	900 nM	
		R	5'-ACA CTG TAA TTG ATG ACC CCA TTC T-3'	900 nM	
		P	5'-HEX-AC CAA GAC T/ZEN/T GTA TGA TGC TGC CAA AGC A-IABkFQ-3'	250 nM	
Hep G Armored RNA (extraction & molecular control)	polyprotein precursor	F	5'-CGG CCA AAA GGT GGT GGA TG-3'	900 nM	50°C 60 min; 95°C 10 min; 40 Cycles: 95°C 30 s, 55°C 60 s 98°C 10 min; 4°C hold
		R	5'-CCC GAC GTC AGG CTC GTC G-3'	900 nM	
		P	5'-FAM-AG GTC CCT C/ZEN/T GGC GCT TGT GGC GAG-IABkFQ-3'	250 nM	

Table S2 | Summary statistics for each parameter measured during 24-hour primary influent sampling at WWTP A and B. Summary statistics are also shown for various transformations of the primary influent SARS-CoV-2 RNA counts.

	Flow (MGD)	BRSV Recovery (%)	PMMoV RNA (CN per L)	SARS-CoV-2 RNA (CN per L)	Recovery Adjusted SARS-CoV-2 RNA (N1 CN per L)	SARS-CoV-2 RNA Load (N1 CN per day)	Recovery Adjusted SARS-CoV-2 RNA Load (N1 CN per day)	SARS-CoV-2 RNA/PMMoV RNA Ratio (log10 N1 CN per L / log10 CN per L)
WWTP A 6-18&19								
$\bar{x}$	15.1	1.89	$7.64x10^{6}$	$1.21x10^{3}$	$3.08x10^{5}$	$7.04x10^{10}$	$1.84x10^{13}$	0.430
s	1.55	3.90	$5.16x10^{6}$	$1.22x10^{3}$	$3.42x10^{5}$	$7.35x10^{10}$	$2.09x10^{13}$	0.057
25th	14.8	0.200	$3.95x10^{6}$	509	$3.69x10^{4}$	$2.96x10^{10}$	$2.09x10^{12}$	0.383
50th	15.7	0.560	$6.45x10^{6}$	667	$1.49x10^{5}$	$3.69x10^{10}$	$9.19x10^{12}$	0.418
75th	16.2	1.70	$8.78x10^{6}$	1490	$5.36x10^{5}$	$8.35x10^{10}$	$3.24x10^{13}$	0.452
CoV (%)	10.2	206	67.5	100	111	104	113	13.3
WWTP A 12-2								
$\bar{x}$	14.8	0.913	$7.91x10^{6}$	$5.82x10^{3}$	$3.13x10^{6}$	$3.19x10^{11}$	$1.75x10^{14}$	0.536
s	1.18	1.49	$3.59x10^{6}$	$4.08x10^{3}$	$2.85x10^{6}$	$2.05x10^{11}$	$1.50x10^{14}$	0.041
25th	13.8	0.075	$6.22x10^{6}$	$2.95x10^{3}$	$7.00x10^{5}$	$1.67x10^{11}$	$4.14x10^{13}$	0.504
50th	15.2	0.15	$6.77x10^{6}$	$4.47x10^{3}$	$2.84x10^{6}$	$2.51x10^{11}$	$1.60x10^{14}$	0.530
75th	15.9	1.40	$10.18x10^{6}$	$8.70x10^{3}$	$4.94x10^{6}$	$4.76x10^{11}$	$2.99x10^{14}$	0.576
CoV (%)	7.97	164	45.4	70	90.8	64.3	85.7	7.70
WWTP B 5-7&8**								
$\bar{x}$	8.46	0.332	$1.13x10^{7}$	213	$8.56x10^{4}$	$6.87x10^{9}$	$2.72x10^{12}$	0.326
s	1.16	0.169	$3.95x10^{6}$	34.6	$6.49x10^{4}$	$1.11x10^{9}$	$1.85x10^{12}$	0.013
25th	7.68	0.185	$7.10x10^{6}$	184	$4.41x10^{4}$	$6.06x10^{9}$	$1.46x10^{12}$	0.316
50th	8.35	0.345	$1.21x10^{7}$	216	$6.26x10^{4}$	$6.48x10^{9}$	$1.99x10^{12}$	0.326
75th	9.47	0.493	$1.47x10^{7}$	244	$1.20x10^{5}$	$8.20x10^{9}$	$4.14x10^{12}$	0.338
CoV (%)	13.7	50.9	34.9	16.2	75.9	16.3	68.1	3.96
WWTP B 12-1&2								
$\bar{x}$	7.98	0.224	$4.29x10^{6}$	$1.51x10^{3}$	$1.65x10^{6}$	$4.58x10^{10}$	$5.37x10^{13}$	0.465
s	1.37	0.274	$1.52x10^{6}$	$1.07x10^{3}$	$1.66x10^{6}$	$3.50x10^{10}$	$5.62x10^{13}$	0.035
25th	6.55	0.060	$2.71x10^{6}$	720	$3.73x10^{5}$	$2.17x10^{10}$	$1.09x10^{13}$	0.431
50th	8.65	0.100	$4.53x10^{6}$	$1.28x10^{3}$	$1.16x10^{6}$	$3.23x10^{10}$	$3.40x10^{13}$	0.459
75th	9.01	0.360	$5.29x10^{6}$	$2.08x10^{3}$	$2.69x10^{6}$	$5.73x10^{10}$	$9.13x10^{13}$	0.500
CoV (%)	17.1	122	35.5	70.5	100	76.4	105	7.53

**SARS-CoV-2 RNA was only detected in 6 of 12 grab samples; non-detects were excluded from summary statistics calculati

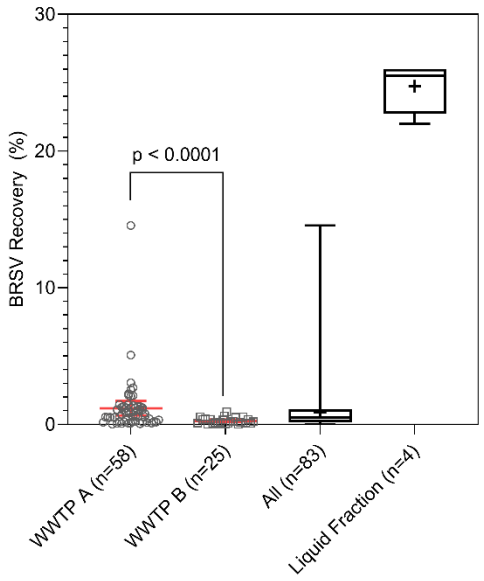

Figure S1 | Process control (BRSV) recovery efficiency for primary influent samples concentrated by adsorption direct-extraction from WWTP A (individual data points, mean and standard deviation), WWTP B (same), and pooled for all primary influent samples. Recovery efficiency for a subset of four primary influent samples concentrated after the suspended solids were removed by centrifugation is also shown. Box plots display minimum, maximum, interquartile range, median, and mean (+). The recovery efficiency from WWTP A was greater than WWTP B ($p < 0.0001$).

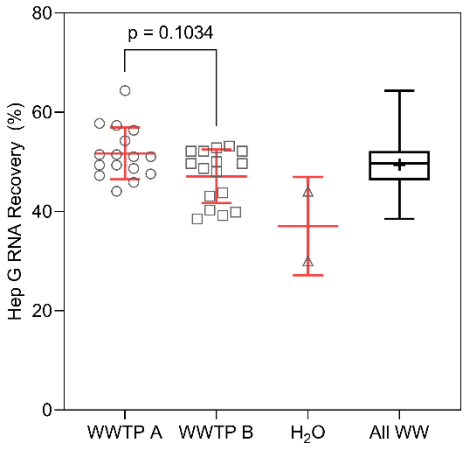

Figure S2 | Recovery efficiency of the HepG extraction and molecular control for primary influent samples concentrated by adsorption direct-extraction from WWTP A (n=16), WWTP B (n=16), PCR-grade water (n=2), and a pooled boxplot of all primary influent samples. Plots for each WWTP and for H_2O display individual data points, mean, and standard deviation. The box plot displays the minimum, maximum, interquartile range, median, and mean (+). There was no difference in the recovery efficiency of the HepG control between primary influent extracts from WWTP A and B ($p = 0.1034$).

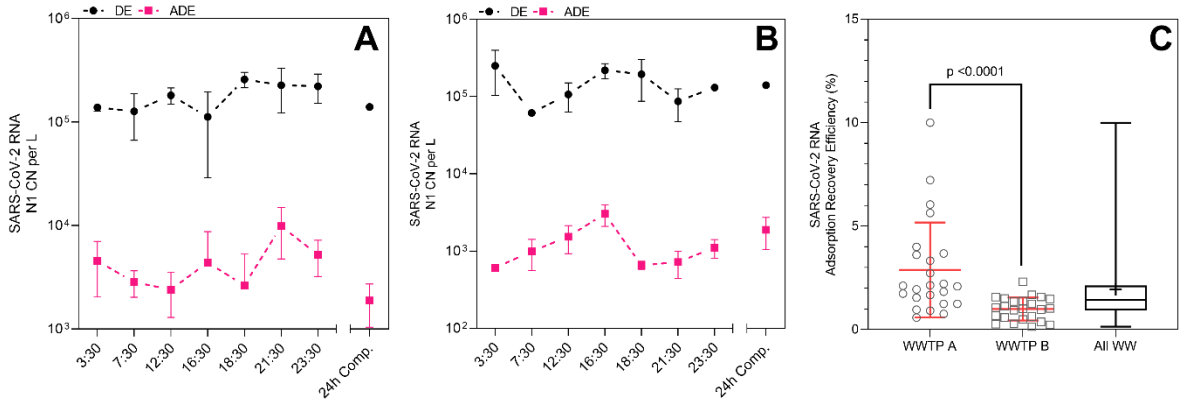

Figure S3 | The mean and standard deviation of SARS-CoV-2 RNA N1 copy number (CN) per liter as measured via direct extraction (DE) of primary influent versus adsorption concentration followed by extraction (ADE) at WWTP A (A) and WWTP B (B) during the 24-hour sampling in December 2020. The SARS-CoV-2 RNA adsorption recovery efficiency was estimated for each WWTP (C) with individual RT-ddPCR data points, mean, and standard deviation at each WWTP shown and a boxplot displaying the minimum, maximum, interquartile range, median, and mean (+) across all RT-ddPCR replicates. SARS-CoV-2 RNA concentration recovery efficiency was significantly greater at WWTP A than WWTP B ($p < 0.0001$).

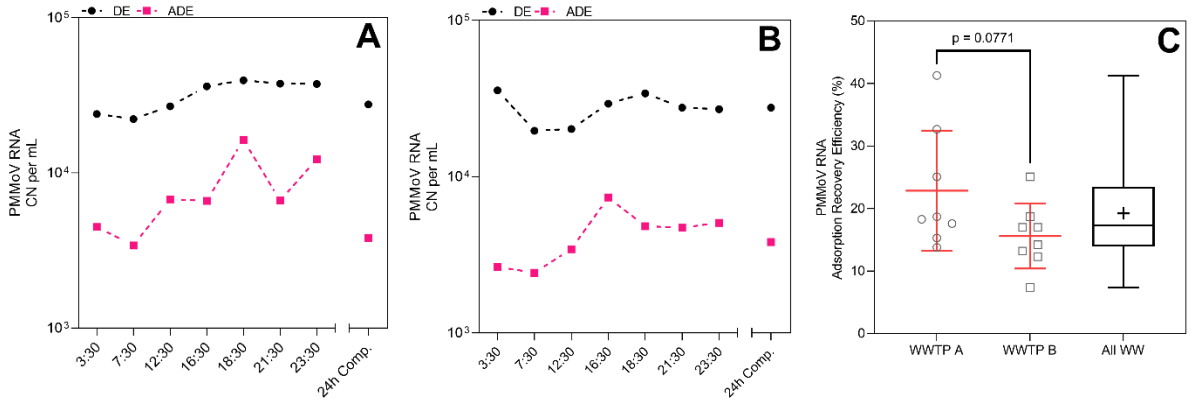

Figure S4 | Mean PMMoV RNA copy number (CN) per milliliter as measured via direct extraction (DE) of influent versus adsorption concentration followed by direct extraction (ADE) at WWTP A (A) and WWTP B (B) during the 24-hour influent sampling in December 2020. The mean and standard deviation of PMMoV RNA adsorption recovery was estimated for each WWTP (C) with individual RT-ddPCR data points, mean, and standard deviation at each WWTP shown and a boxplot displaying the minimum, maximum, interquartile range, median, and mean (+) across all RT-ddPCR replicates. PMMoV RNA concentration recovery efficiency was similar (p = 0.0771) between the two WWTPs.

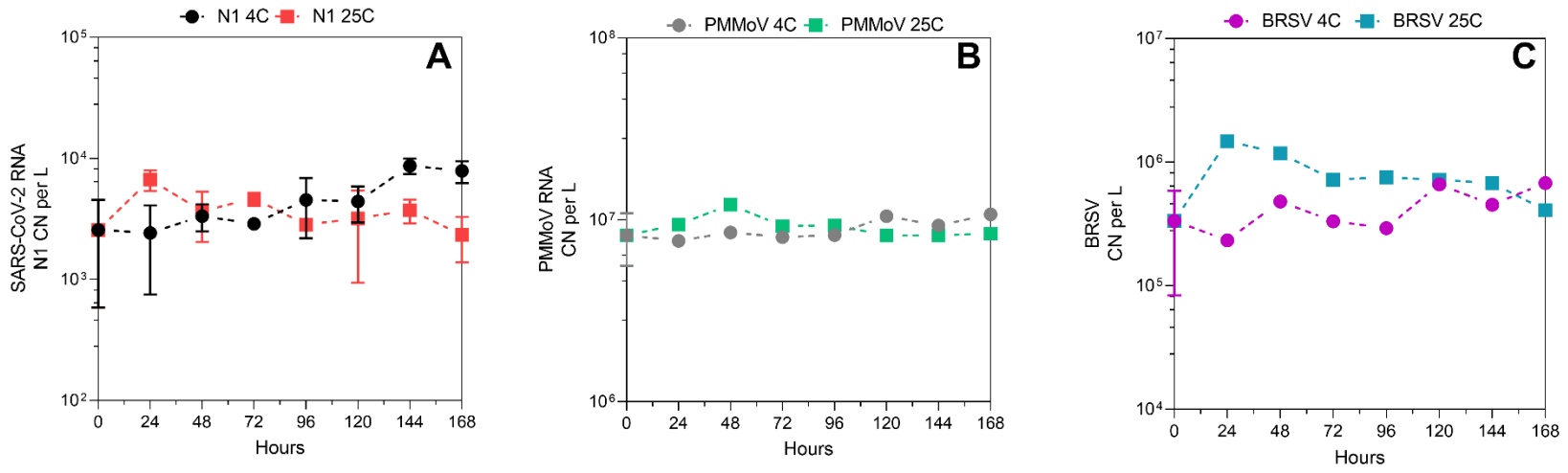

78

79 Figure S5 | SARS-CoV-2 RNA N1 copy number (CN) per liter (A), PMMoV RNA CN per liter (B), and BRSV RNA CN per liter (C)
80 enumerated every 24 hours over 7 days (168 hours) of incubation at 4°C and 25°C in primary influent from WWTP A. Plots display
81 mean and standard deviation (where possible).

82

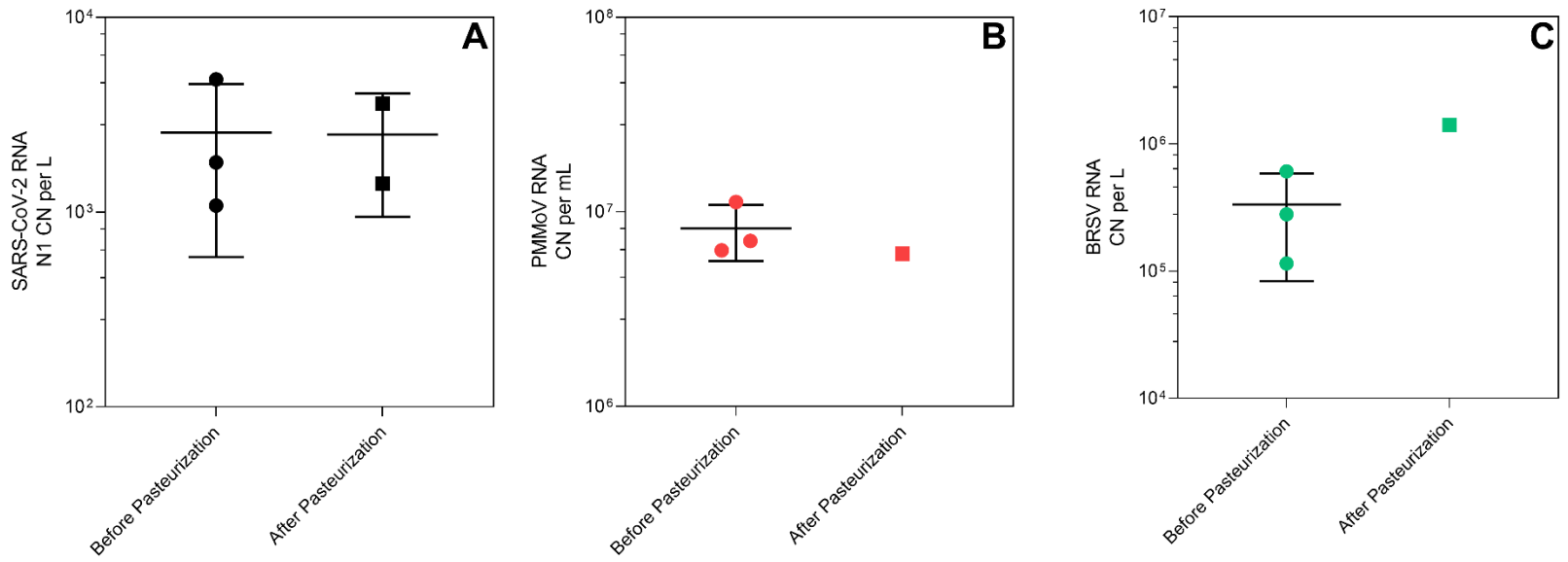

Figure S6 | Measurements of SARS-CoV-2 RNA N1 CN per liter (A), PMMoV RNA CN per liter (B), and BRSV RNA CN per liter (C) before and after pasteurization for 90 minutes at 60°C in primary influent from WWTP A. Plots display individual replicate measurements, mean, and standard deviation (where available).

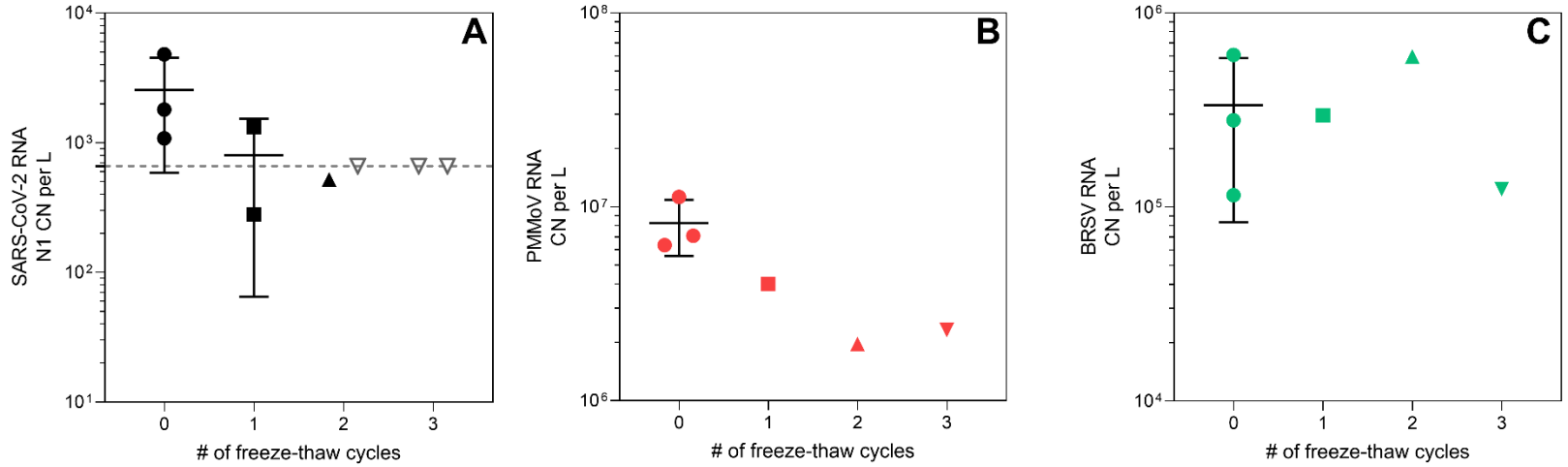

Figure S7 | Measurements of SARS-CoV-2 RNA N1 CN per liter (A), PMMoV RNA CN per liter (B), and BRSV RNA CN per liter (C) following sequential freeze-thaw cycles of primary influent from WWTP A. Plots display individual replicate measurements, mean, and standard deviation (where available).

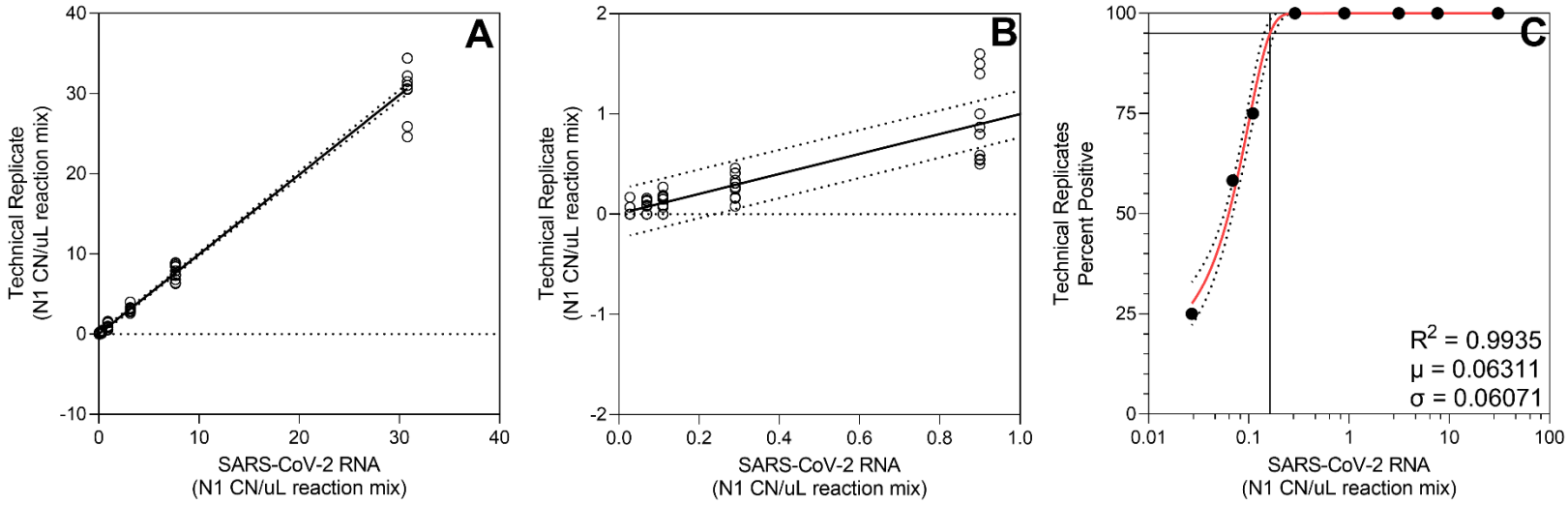

93

94 Figure S8 | Quantification of SARS-CoV-2 RNA N1 copy numbers in RT-ddPCR technical replicates along a 1:3 dilution series of RNA
95 positive control material (A,B). A Gaussian distribution fit to the proportion of positive technical replicates along the dilution series (C)
96 and used to estimate the N1 95% LOD of 3.3 copies (95% CI: 2.8 – 3.8) per RT-ddPCR reaction.

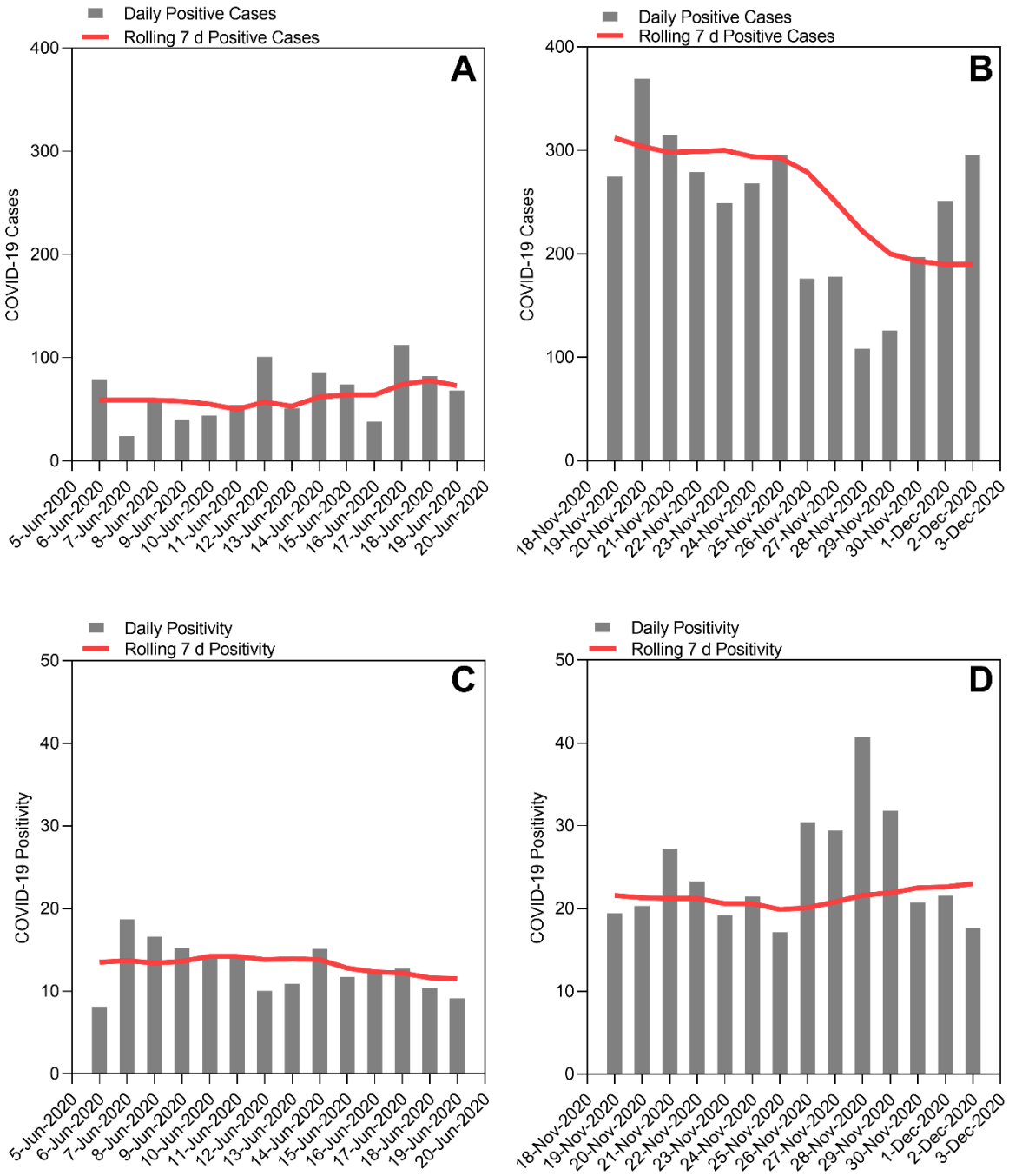

Figure S9 | Daily new cases, positivity, and their associated 7-day rolling averages for COVID-19 in the county containing WWTP A during the two weeks immediately prior to 24-hour influent sampling on June 18 and 19, 2020 (A & C) and December 2, 2020 (B & D).

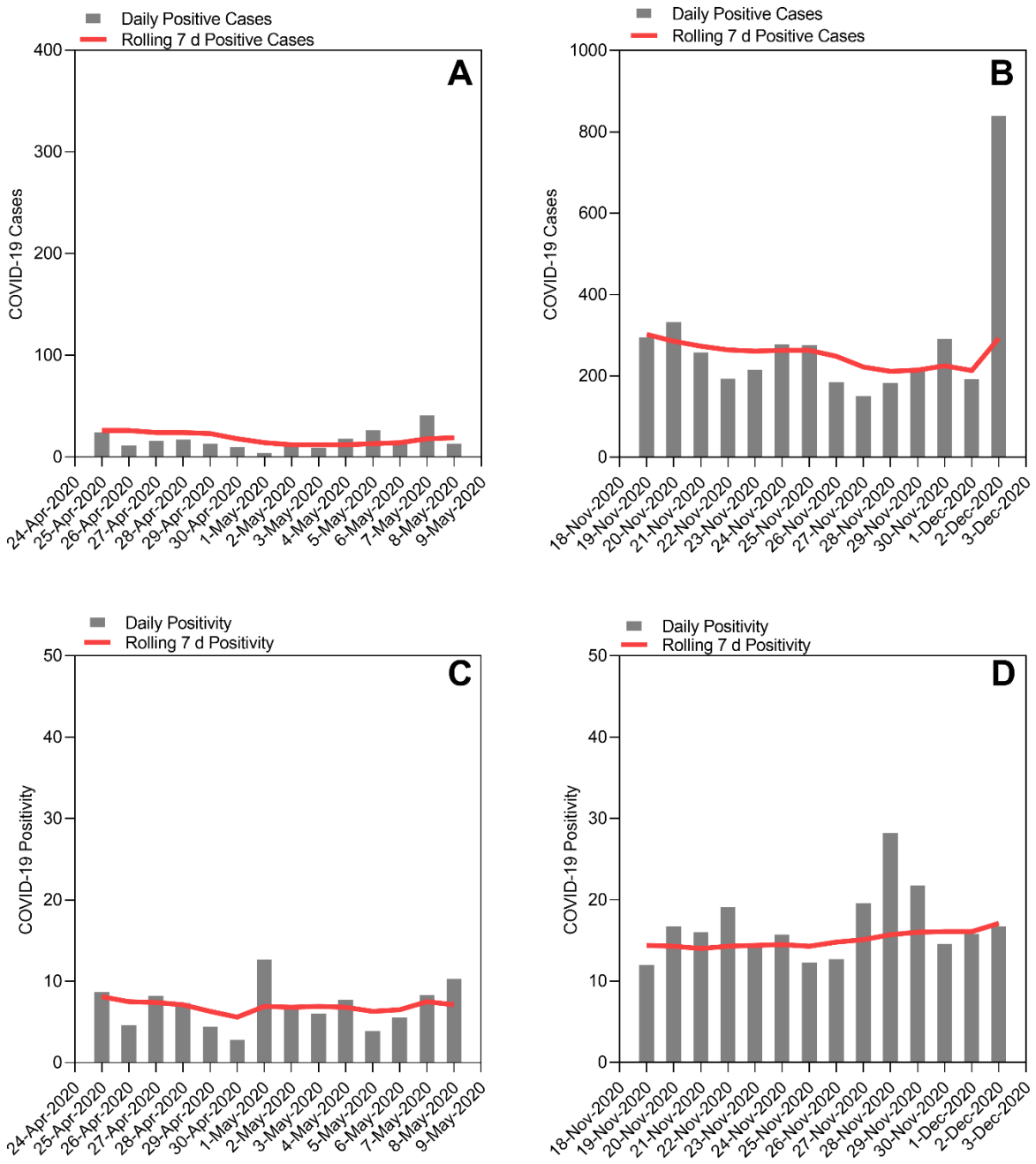

Figure S10 | Daily new cases, positivity, and their associated 7-day rolling averages for COVID-19 in the county containing WWTP B during the two weeks immediately prior to 24-hour influent sampling on May 8 and 19, 2020 (A & C) and December 1 and 2, 2020 (B & D).

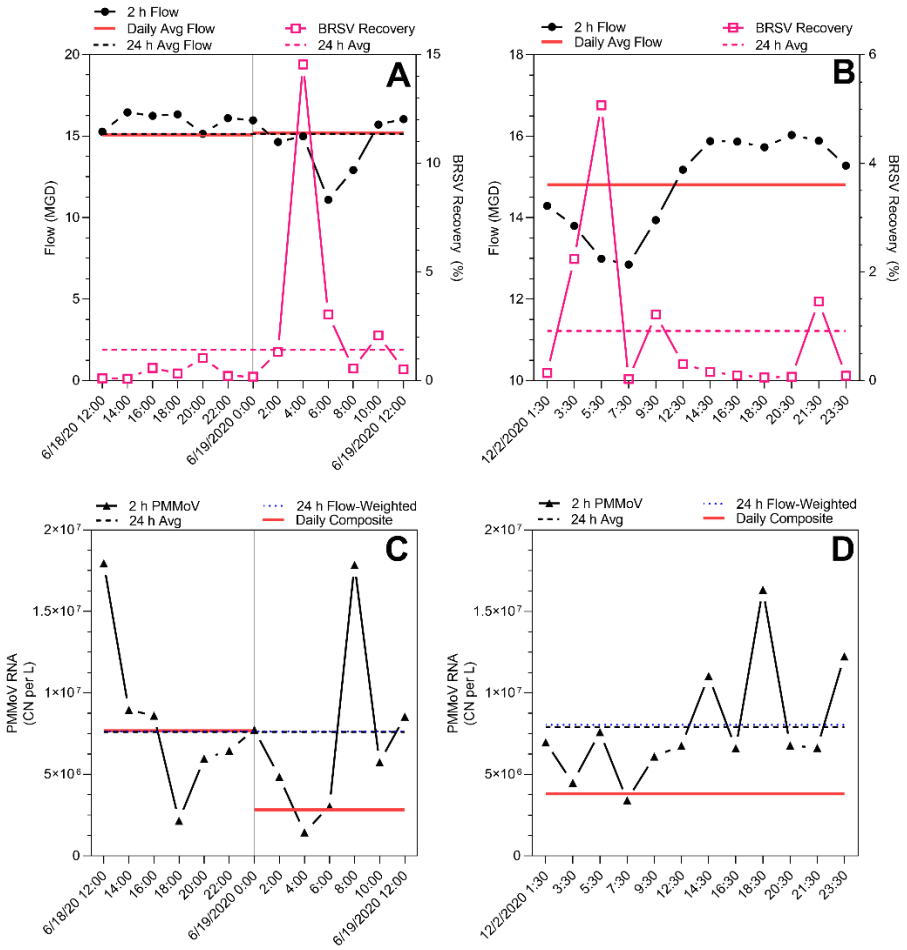

107

108 Figure S11 | WWTP A primary influent characteristics as observed during two 24-hour sampling
109 events: influent flow rates and process control recovery efficiency (A & B), and PMMoV RNA copy
110 number density (C & D). Data displayed include the observations in serial grab samples, the
111 average observed over the 24-hour interval, the flow-weighted 24-hour average, and the daily
112 composite sample observation (when available).

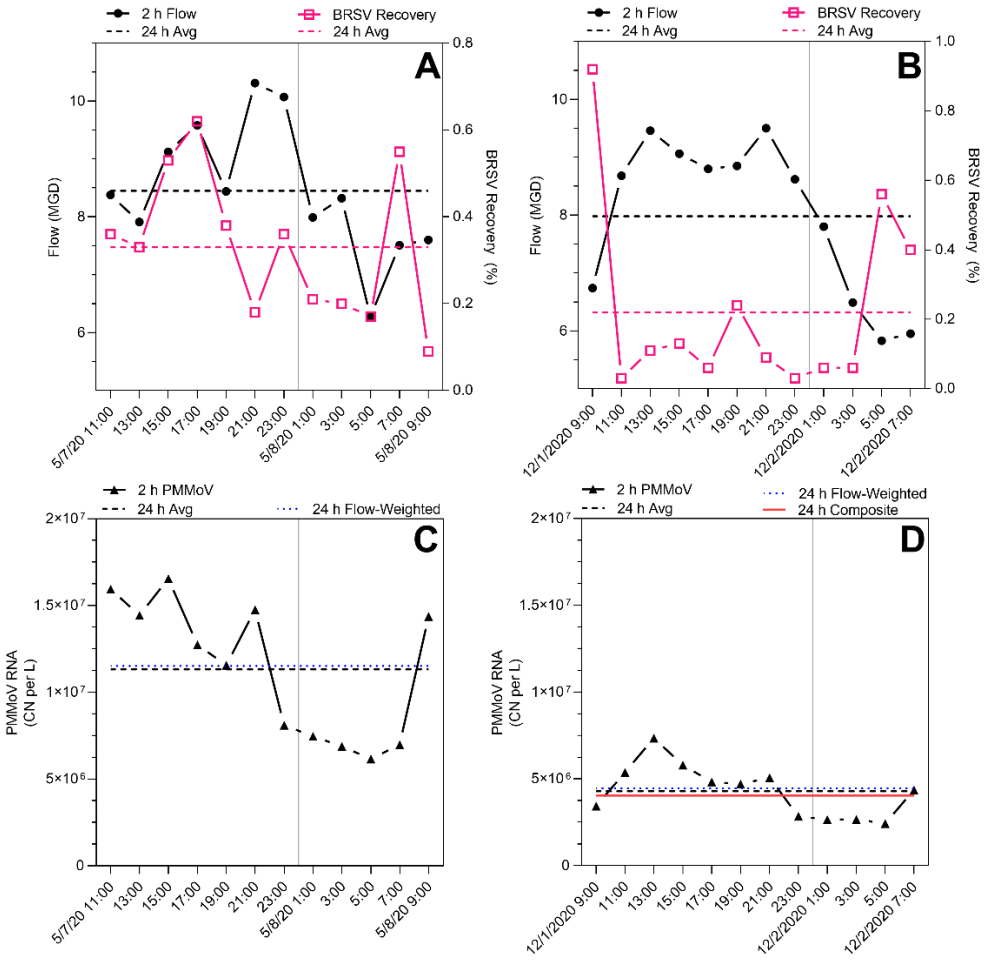

Figure S12 | WWTP B primary influent characteristics as observed during two 24-hour sampling events: influent flow rates and process control recovery efficiency (A & B), and PMMoV RNA copy number density (C & D). Data displayed include the observations in serial grab samples, the average observed over the 24-hour interval, the flow-weighted 24-hour average, and the daily composite sample observation (when available).

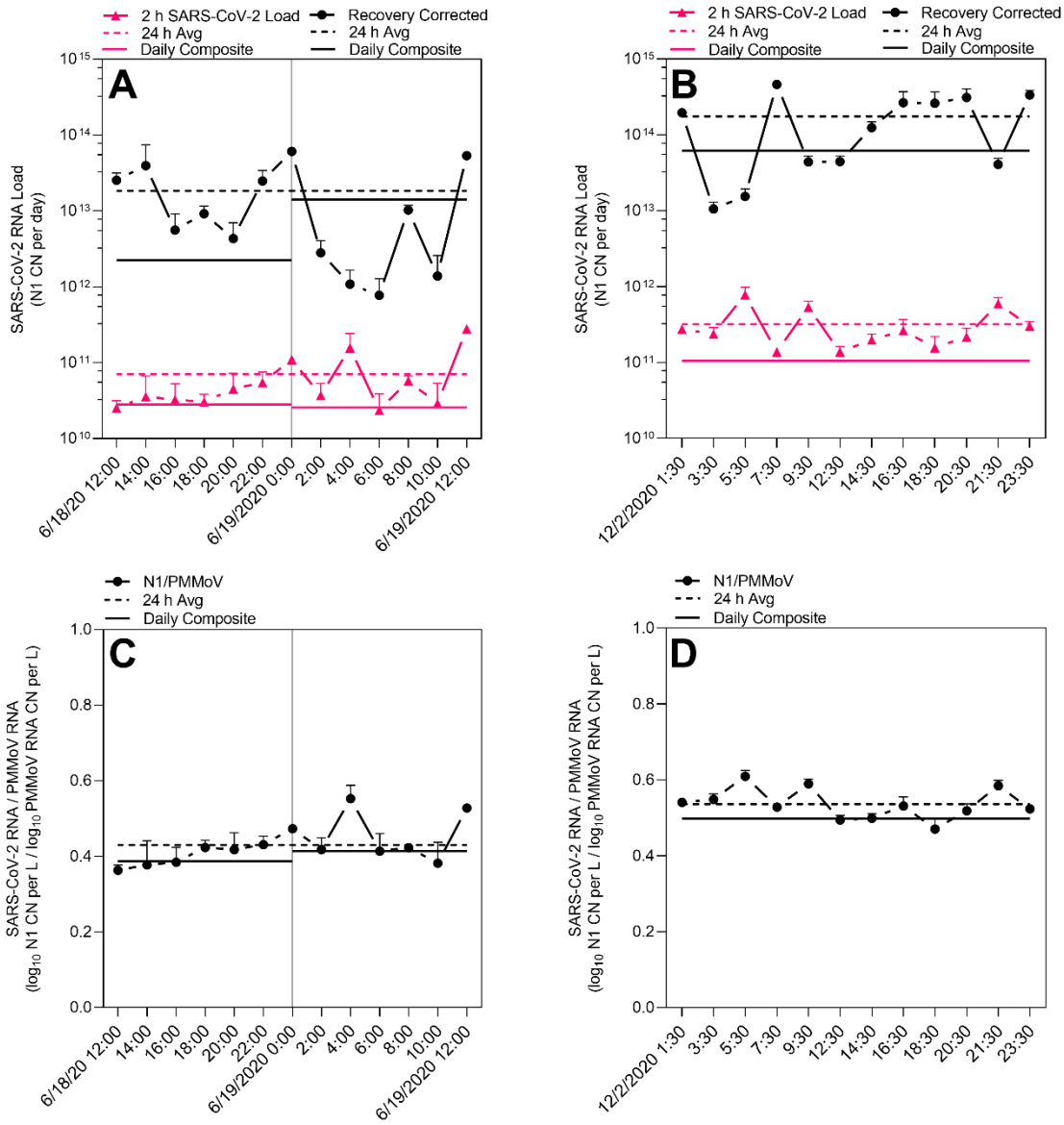

Figure S13 | WWTP A primary influent characteristics as measured during two 24-hour sampling events: influent SARS-CoV-2 loading, copy number (CN) per day (concentration x flow), with and without recovery adjustment (A & B), and the ratio of the $\log_{10}$ SARS-CoV-2 RNA copy number per liter to $\log_{10}$ PMMoV RNA copy number per liter (C & D). Data displayed include the observations in serial grab samples, the average observed over the 24-hour interval, and the daily composite sample observation (when available).

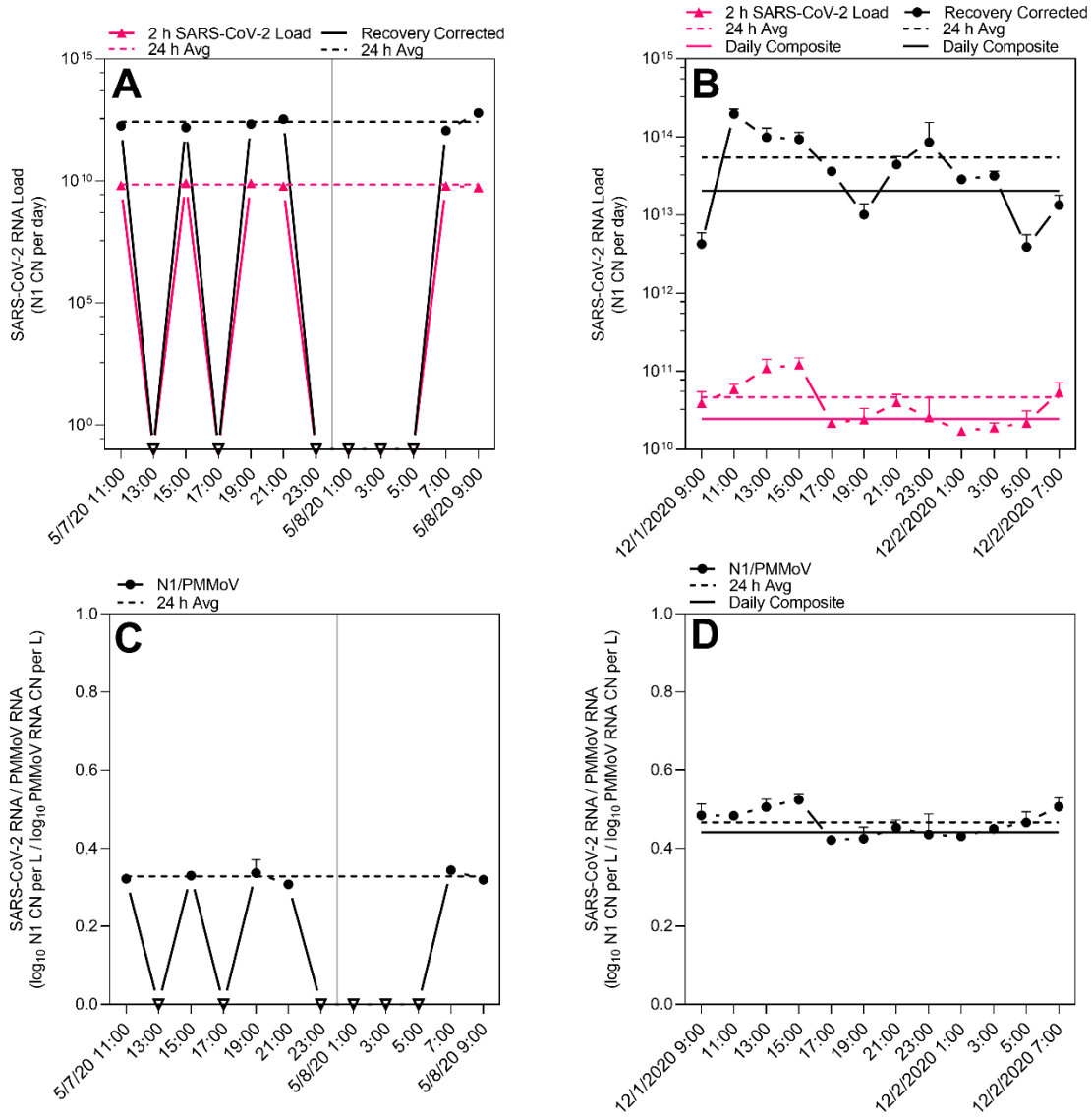

126

127 Figure S14 | WWTP B primary influent characteristics as measured during two 24-hour sampling
128 events: influent SARS-CoV-2 loading, copy number (CN) per day (concentration x flow), with and
129 without recovery adjustment (A & B), and the ratio of the $\log_{10}$ SARS-CoV-2 RNA copy number
130 per liter to $\log_{10}$ PMMoV RNA copy number per liter (C & D). Data displayed include the
131 observations in serial grab samples, the average observed over the 24-hour interval, and the daily
132 composite sample observation (when available).

133

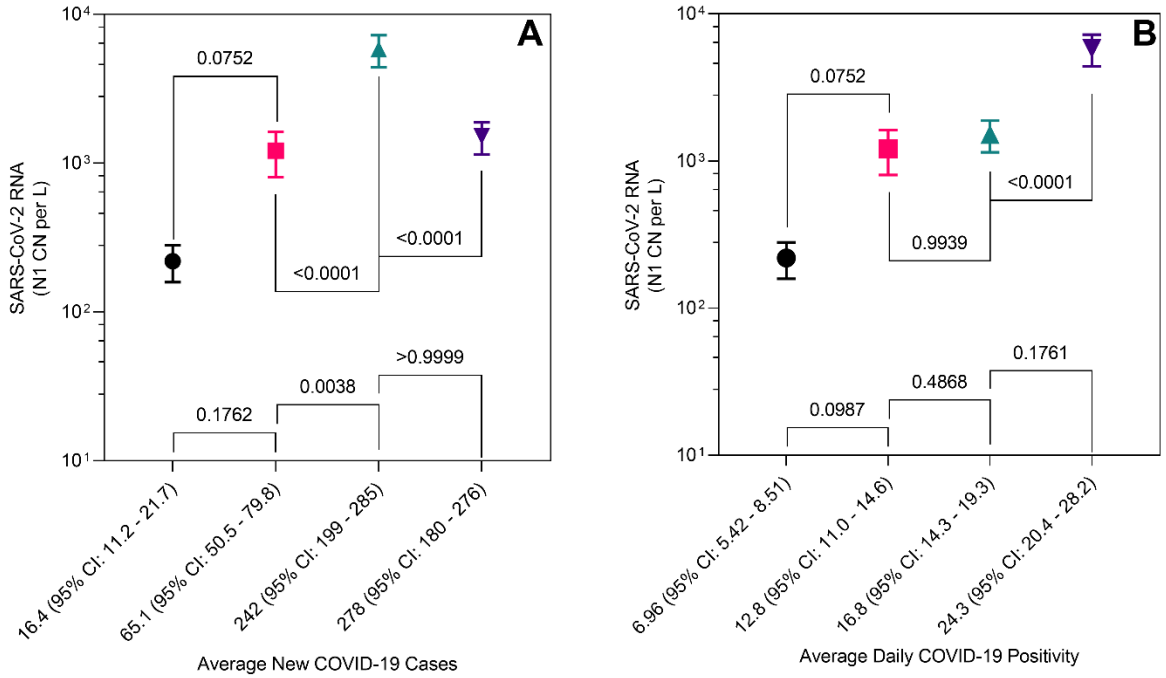

Figure S15 | SARS-CoV-2 RNA N1 concentrations, copy number (CN) per liter, in primary influent stratified by ordinal arrangement of average daily COVID-19 cases (A) and average daily COVID-19 positivity (B). Clinical averages and confidence intervals are calculated for the two weeks prior to the 24-hour primary influent sampling period.